JOURNAL OF AEROSPACE COMPUTING, INFORMATION, AND COMMUNICATION
Vol. 4, March 2007

Calculation Verification: Pointwise Estimation of Solutions and Their Method-Associated Numerical Error

David Palmer Smitherman* , James R. Kamm† , and Jerry S. Brock‡
Los Alamos National Laboratory, Los Alamos, NM 87545

Calculation verification is a method of quantifying the convergence properties of a specific implementation of an algorithm without using an exact solution, whereas code verification does use an exact solution. Calculating global convergence while performing calculation verification can be problematic as no exact solution is generally available. A second difficulty sometimes encountered in both code and calculation verification is when the computed solutions at a point in space converge in an oscillatory manner, making calculation of convergence difficult. An extension to the standard method of calculation and code verification is explored which may address both of these issues. The proposed method uses pointwise convergence analysis to estimate global convergence behavior by first estimating a discrete solution to the partial differential equations. The estimated solution is then used in place of an exact solution to evaluate global convergence rates when conducting a calculation verification analysis. Additionally, the absolute value of the pointwise error is calculated, allowing for monotonic or oscillatory convergence. This method was tested on four pure hydrodynamics problems using the Eulerian code RAGE. A linear acoustic wave and a 1-D Riemann problem both have exact mathematical solutions, which were compared to the estimated solution. For these two problems both code and calculation verification methods were applied. A nonlinear acoustic wave and 2-D Riemann problem both have no exact solutions, but the estimated solution was shown to be useful in providing a more accurate solution on a coarse grid than the calculated solution. For these two problems, only a calculation verification analysis was conducted.

Nomenclature

A	convergence prefactor
E	specific total energy
e	specific internal energy (SIE)
k	wavevector
N_x, N_y	total number of cells in the x or y spatial dimensions
p	pressure
q	convergence rate
t	time
u	scalar speed
u_x, u_y	velocity in x or y
x, y	spatial dimensions

Received 22 March 2006; accepted for publication 26 December 2006.

* Staff Member, P.O. Box 1663, SB-CS, MS F691, AIAA Member. dps@lanl.gov
† Staff Member, P.O. Box 1663, X-1-MV, MS B259, AIAA NonMember. kammj@lanl.gov
‡ Staff Member, P.O. Box 1663, X-1-MV, MS B259, AIAA Member. jsbrock@lanl.gov

γ	ideal gas constant
Δx, Δy	arbitrary computational spatial scale
ε	small perturbation parameter
$\hat{\xi}$	estimated solution
ξ^*	exact solution
ξ_c, ξ_m, ξ_f	computational solution with course, medium, or fine spatial zoning
$\xi_{\Delta x}$	computational solution with arbitrary spatial zoning
ρ	density
σ	spatial zoning ratio
ω	temporal frequency

I. Introduction

WHEN a code is written to provide approximate numerical solutions of partial differential equations (PDE), one frequently wishes to know the convergence properties of the specific implementation of the algorithm that has been chosen. Comparison of the realized and theoretical convergence rates may then be made. Confirming that the implementation of an algorithm actually converges and is reasonably close to theoretical values gives one confidence that the algorithm has been implemented correctly. In addition, convergence rates may be used in order to estimate how fine the mesh needs to be in order solve certain problems to the desired accuracy.

Two types of mesh convergence analysis will be discussed here. *Code verification* provides an analysis of the error between computed and exact solutions for well-defined problems.[1-6] In order to conduct code verification, one must assume a mathematical model for the discretization error; equally important is the further supposition that an exact solution can be evaluated for the problem of interest. *Calculation verification* also quantifies convergence using an error model but without an exact solution. Both code and calculation verification provide quantitative convergence rates for a code on the problem of interest.

Because calculation verification is usually performed on complex problems with no exact solution, pointwise convergence rates are easily calculated, but global convergence rates are more difficult to calculate. Nevertheless, global convergence rates are a desirable and important aspect of any verification analysis. Our primary objective is to explore a new method by which global convergence rates may be estimated in the case where no exact solution is known. As a consequence of calculation verification, a pointwise *estimation* of the solution to the continuous equations is constructed. Global convergence rates may then be approximated using this estimated solution in place of an exact solution. This approach could be coupled with uncertainty analysis methods[5,7,8] to provide estimates of the computational error from numerical discretization.

A second difficulty sometimes encountered during both code and calculation verification is when oscillatory convergence is encountered. By oscillatory convergence, we are referring to the case where the computational solution at a point in the mesh approaches the exact solution as the zoning is refined, but with some computational results of magnitude greater than and others of magnitude smaller than the exact solution. In this investigation, we modify the standard error model to allow calculation of oscillatory convergence, giving a more complete analysis. This approach may be particularly useful in situations that could contain a large number of oscillatory converging points, such as discontinuities (e.g., shocks). Instead of solving the error model analytically, we solve it using Newton's method; this approach allows for a more complex error model, if desired.

Both code and calculation verification analyses were performed on two hydrodynamic test problems with exact solutions using the new method. The convergence of two additional problems without exact solutions was determined using calculation verification only. Because we use the estimated solution to calculate an approximation to the global error when no exact solution is available, we explore the accuracy of the estimated solution by comparing it to the exact solution in the first two problems mentioned. Two of the test problems have discontinuities, at least one of which exhibited points with oscillatory convergence. The new methodology successfully incorporated the oscillatory convergence rate of these points into a global convergence rate.

Our goal is to demonstrate that one may (1) approximate global convergence rates using the estimated solution when no exact solution is known, and (2) calculate oscillatory convergence and include this data into a global convergence analysis. Although the "simple" or "idealized" applications we consider are restricted to the dynamics

of a single, inviscid, non-heat-conducting, polytropic gas, the method we develop applies more generally to numerical solutions of space- and time-dependent PDEs.

This paper is structured as follows. In § 2 we review mesh convergence analysis. We extend those concepts in § 3 and provide examples of the new approach in § 4. A summary of our findings is presented in § 5. A more complete compilation of results of this approach may be found in Ref. [9].

II. Mesh Convergence Analysis

Throughout this report we consider the evaluation of the numerically computed solutions to PDEs that depend on both space $\boldsymbol{x}$ and time t. We refer to an exact solution that is calculated from the error model as an estimated solution and designate it by $\hat{\xi}$. For the moment, we assume that the exact solution, ξ^*, is unknown and that the standard model regarding the behaviour of pointwise discretization error is given by,[5]

$$\hat{\xi} - \xi_{\Delta x} = A\Delta x^q \tag{1}$$

which comes from assuming a power series expansion for discretization error.

The symbol $\xi_{\Delta x}$ is the computed solution obtained on a grid with characteristic discrete spatial scale Δx. The spatial convergence rate is designated q, and A is the corresponding convergence prefactor. Because Eq. (1) is written pointwise, all variables, except Δx, are functions of space and time. Implicit with Eq. (1) is the assumption that all computational solutions, $\xi_{\Delta x}$, are contained within the regime of asymptotic convergence, consistent with the error model. Additionally, a fixed spatial grid and time step are assumed for Eq. (1) to be valid, with no spatial or temporal refinement as the simulation proceeds. For multiple dimensions, the spatial discretization is equal along all dimensions, which are then all equated to Δx. This assumes that the order of spatial accuracy is identical in all dimensions, which may or may not be true.

Although Eq. (1) may not be used with non-uniform zoning, the new verification procedure presented here should be directly applicable to non-uniform zoning by spatially weighting the error from various sized cells when calculating global convergence. An error model other than Eq. (1) that accounted for the non-uniform zoning would be required. Ref. [10] provides an example of convergence analysis with non-uniform grids.

A more general error model than Eq. (1) could include terms from all spatial dimensions, temporal errors, and cross terms.[11-14] Because the numerical method may or may not converge precisely to the exact solution of the continuous equations, a zeroth-order error, which is not included in Eq. (1), may be present. Likewise, higher order terms may have some influence on the total error. Thus, although the convergence rates presented in this paper may not be as accurate as possible, our verification procedure could certainly be used with a more complex error model than Eq. (1) . Nevertheless, as the purpose of this paper is to explore improvements to code and calculation verification methodology, and not to obtain exact convergence results, we have consciously chosen a simple error model in order to focus on the method itself. If a more difficult initial application for the new method had been selected, such as one comprised of variable mesh spacing, spatial and temporal error analysis, and multiphysics simulations instead of simply hydrodynamics, then failure of the model would have resulted in confusion over whether the difficulty lay in the complexity of application or the new method itself. Eq. (1) was believed to be sufficient for our current purposes based on previous experience. More complex error models could have entailed additional variables requiring an unnecessary number of calculations for this study.

The estimated solution in Eq. (1) effectively absorbs all error terms that have been neglected in the error model. Therefore, the nature of the estimated solution, which is *not* equivalent to an exact solution, depends on the error model selected. Because of the simplicity of Eq. (1), the difference between the estimated and exact solutions may be a relatively large value in the test problems that we present.

The unknowns in Eq. (1) are $\hat{\xi}$, A, and q. Three calculations of coarse (c), medium (m), and fine (f) zoning completely specify a solution for Eq. (1),

$$\hat{\xi} - \xi_c = A\Delta x_c^q, \quad \hat{\xi} - \xi_m = A\Delta x_m^q, \quad \hat{\xi} - \xi_f = A\Delta x_f^q \tag{2}$$

An important aspect of the analysis is the mapping of computational solutions onto the same grid. In order to solve Eqs. (2), all calculated values must be mapped onto the coarse grid by spatial averaging. Assuming that the

zoning ratios, σ , are the same,

$$\Delta x_c = \sigma \Delta x_m = \sigma^2 \Delta x_f \tag{3}$$

For the convergence rate, the solution to Eqs. (2) is

$$q = \log\left(\frac{\xi_m - \xi_c}{\xi_f - \xi_m}\right) / \log(\sigma) \tag{4}$$

One possible formulation used to compute A and $\hat{\xi}$ is

$$A = \frac{\xi_f - \xi_m}{\Delta x_f^q(\sigma^q - 1)}, \quad \hat{\xi} = \xi_f + A\Delta x_f^q(\sigma^q - 1) \tag{5}$$

Eqs. (4–5) may be used in calculation verification analysis.

When the exact solution, ξ^*, is known, code verification analysis may be performed. In this case, only two computational solutions are required to solve Eq. (1) and the pointwise convergence relations of Eqs. (2) become,

$$\xi^* - \xi_c = A\Delta x_c^q, \quad \xi^* - \xi_f = A\Delta x_f^q \tag{6}$$

The solutions to Eqs. (6) are

$$q = [\log(\xi^* - \xi_c) - \log(\xi^* - \xi_f)]/\log(\sigma), \quad A = (\xi^* - \xi_c)/\Delta x_c^q \tag{7}$$

When considering discretized fields of continuum variables, *e.g.*, computed solutions to the PDEs, we propose approximating global convergence rates using the estimated pointwise solution in place of the exact solution as a part of calculation verification. The estimated solution is now considered to be a known quantity as we calculate it first from the pointwise convergence relations, Eqs (4–5) above. Global norms may then be approximated for problems with no exact solution. Incorporating the estimated solution into the standard global norm,

$$\|\hat{\xi} - \xi_{\Delta x}\|_\alpha \equiv \left(\sum_{i=1}^{N} |\hat{\xi}(x_i, t_i) - \xi_{\Delta x}(x_i, t_i)|^\alpha\right)^{1/\alpha} \tag{8}$$

where α is some integer. The equations for global convergence are then written

$$\|\hat{\xi} - \xi_c\|_\alpha = A_g \Delta x_c^{q_g}, \quad \|\hat{\xi} - \xi_f\|_\alpha = A_g \Delta x_f^{q_g} \tag{9}$$

The g subscript on the convergence rate and prefactor is a reminder that these are global values that are functions of time, but not of space. The solutions to Eqs. (9) are,

$$q_g = [\log\|\hat{\xi} - \xi_c\|_\alpha - \log\|\hat{\xi} - \xi_f\|_\alpha]/\log(\sigma^2), \quad A_g = \|\hat{\xi} - \xi_c\|_\alpha / \Delta x_c^{q_g} \tag{10}$$

The equations for global convergence and their solutions with a known exact solution (code verification) are analogous to the global case with the estimated solution, Eqs. (9–10), only the estimated solution is replaced by the exact solution.

III. Extended Mesh Convergence Analysis

For a numerical method that is pointwise convergent, the computational error must decrease as zone size decreases. The relationship between the estimated (or exact) solution at a specific point in space and the computational results

from the different mesh resolutions must be,

$$|\hat{\xi} - \xi_c| > |\hat{\xi} - \xi_m| > |\hat{\xi} - \xi_f| \geq 0 \tag{11}$$

At any point in the mesh, the magnitude of the physical variables output by the simulation, ξ_c, ξ_m, and ξ_f may be in one of six possible sequences. In the two cases where the coarse calculation value is intermediate, *viz.*,

$$\xi_m \geq \xi_c \geq \xi_f \text{ or } \xi_f \geq \xi_c \geq \xi_m \tag{12}$$

there is no value for the estimated solution that satisfies Eq. (11), so the simulation results are not converging; likewise, there is no solution for Eqs. (4–5) in this case. If the simulation values are increasing with Δx such that

$$\xi_f < \xi_m < \xi_c \tag{13}$$

then Eqs. (4–5, 11) are valid and the solution space for the estimated solution, from Eq. (11), is

$$\hat{\xi} \leq \xi_f \tag{14}$$

If the simulation values are decreasing with Δx, then the ordering of the simulation values and the solution space for the estimated solution are respectively given by,

$$\xi_f > \xi_m > \xi_c, \quad \hat{\xi} \geq \xi_f \tag{15}$$

We refer to the previous two cases as monotonic convergence. Two possibilities remain, which represent oscillatory convergence. They and their solution spaces for the estimated solution are

$$\begin{aligned} &\xi_m > \xi_f > \xi_c, && \frac{\xi_m + \xi_f}{2} > \hat{\xi} > \frac{\xi_m + \xi_c}{2} \\ &\xi_c > \xi_f > \xi_m, && \frac{\xi_m + \xi_f}{2} < \hat{\xi} < \frac{\xi_m + \xi_c}{2} \end{aligned} \tag{16}$$

Equations (16) meet the test of convergence given by Eq. (11) and, so, would seem to represent a valid, pointwise convergence case not admitted by Eqs. (4–5). As most computational cells in simulations of physical relevance do not exhibit oscillatory convergence, calculating monotonic convergence alone has proven an acceptable method for the majority of mesh convergence studies. Oscillatory convergence may occur in some problems, e.g., at shock and discontinuity boundaries, and may therefore be important for mesh convergence analysis of non-smooth problems. As our procedure highlights using the discrete estimated solution to approximate the global convergence rate as shown by Eqs. (8–10), calculating the estimated solution for every point in the mesh, including oscillatory converging points, is an important aspect of this method, irrespective of the error model.

In order to allow for pointwise oscillatory as well as monotonic convergence, we modify the error model by taking the absolute value of the error. Following the original approach, we assume that the absolute error may be expanded in a power series giving the relations,

$$|\hat{\xi} - \xi_c| = A\Delta x_c^q, \quad |\hat{\xi} - \xi_m| = A\Delta x_m^q, \quad |\hat{\xi} - \xi_f| = A\Delta x_f^q \tag{17}$$

These equations can no longer be easily solved analytically. Instead, a convergence analysis code was written to solve them using Newton's method[15] to simultaneously solve for $\hat{\xi}$, A, and q. Derivatives were analytically determined with the derivative for the absolute value with an argument of zero selected to be zero. An advantage of using Newton's method is that it allows for the solution of as complex an error model as desired.

Taking the full Newton step while solving Eqs. (17) was found to be inadvisable as few points converged; implementation of an algorithm to optimize the Newton step resolved this difficulty.[16] Assignment of an appropriate initial value for the array of unknowns to be used in the iterative solver is important. If the fine grid computational

solution was located within the allowable solution space for the estimated solution as described by Eqs. (14–16), then the starting point for the estimated solution was chosen to be the fine grid solution,

$$\hat{\xi}^{(0)} = \xi_f \tag{18}$$

where the superscript indicates the iteration index. If the fine grid solution was not within the estimated solution's predicted solution space, which may occur with oscillatory convergence as described by Eqs. (16), then starting at the fine grid solution did not always yield convergence of the Newton method. Instead, the initial prediction for the estimated solution was initialized by calculating the center of the solution space defined by Eqs. (16),

$$\hat{\xi}^{(0)} = \frac{1}{4}(\xi_c + 2\xi_m + \xi_f) \tag{19}$$

With $\hat{\xi}^{(0)}$, initial values for the other two unknowns were obtained,

$$A^{(0)} = |\hat{\xi}^{(0)} - \xi_c|/\Delta x_c^{q^{(0)}}, \quad q_i^{(0)} = [\log|\hat{\xi}^{(0)} - \xi_c| - \log|\hat{\xi}^{(0)} - \xi_m|]/\log(\sigma) \tag{20}$$

The solution to Eqs. (17) for $\hat{\xi}$, A, and q were then determined using iterations of the Newton method. The procedure was followed at each cell of the computational mesh.

Although most grid points converged, a few did not for a variety of reasons. First, at certain points the ordering of the function values was inconsistent with the assumption of the error model as described by Eq. (13). A trap was inserted into the code to find and eliminate these points from the analysis. Second, non-convergence follows if ξ_c, ξ_m, and ξ_f are all nearly equal. A second trap was used to find these points and remove them from the analysis as well. Only points that presented values for ξ_c, ξ_m, and ξ_f consistent with convergence and with magnitudes distinct from one another (beyond a user specified tolerance) were analyzed by the Newton solver. The third difficulty was with the Newton solver itself, as the method sometimes produced a zero element on the diagonal of the upper triangular matrix yielding a non-invertible, ill-conditioned matrix. Most of the time this difficulty could be overcome by simply assigning a minimum value to the diagonal elements, but the price of such a procedure was to eliminate the certainty that the Newton step was indeed in a direction that reduced the total error.

Convergence criteria for the solver included both the fractional change in the variables with each step and the total error in Eqs. (17); these values were generally on the order of 10^{-12} to 10^{-15}. If the solver failed to converge on a few points in a particular problem, a reduction in the tolerance of the convergence criteria was made until all points either converged or did not in fewer than 100 Newton iterations. Experimentation with code parameters showed that increasing the maximum number of Newton solver iterations did not usually result in all the points converging, while lowering the tolerance did. The mesh points at which convergence was not obtained were flagged and not included in the subsequent global analysis.

IV. Results and Interpretation

The technique described above was applied to a set of compressible hydrodynamics problems. The governing equations for these problems are the Eulerian-frame equations for the dynamics of a single, inviscid, non-heat-conducting gas, describing the conservation of mass, momentum, and total energy as:

$$\begin{aligned} \frac{\partial \rho}{\partial t} + \frac{\partial}{\partial x}(\rho u_x) &= 0 \\ \frac{\partial(\rho u_x)}{\partial t} + \frac{\partial}{\partial x}(\rho u_x^2 + p) &= 0 \\ \frac{\partial(\rho E)}{\partial t} + \frac{\partial}{\partial x}(\rho E u_x + p u_x) &= 0 \end{aligned} \tag{21}$$

In these equations, ρ is the density, u_x is the x-velocity, p is the thermodynamic pressure, and

$$E = (1/2)u^2 + e \tag{22}$$

Table 1 Four test problems were used.

	Exact solution known	Exact solution unknown
Smooth solution	2-D linear acoustic wave	2-D nonlinear acoustic wave
Discontinuous solution	1-D Riemann problem	2-D Riemann problem

is the specific total energy, where e is the specific internal energy (SIE). We assume the polytropic gas equation of state

$$p = (\gamma - 1)\rho e \tag{23}$$

where γ is the adiabatic exponent.

The four problems presented in Table 1 were used as test problems. We chose this set of problems as it offers a mixture of solution properties that spans the issues of smooth and discontinuous solution behavior with and without an exact solution.

We used the RAGE[17] hydrodynamics code to perform the numerical simulations. RAGE is an adaptive mesh refinement (AMR) hydrodynamics code that uses a high-order Godunov (direct Eulerian, piecewise linear) method with an approximate Riemann solver to obtain the solution of the gas dynamics equations. We only considered 1-D and 2-D Cartesian geometries in the problems that were evaluated. The calculations that we performed with RAGE were all run on uniform, non-AMR grids. All simulations were run with constant, fixed time steps; moreover, identical time steps were used for meshes with different zonings on the same problem. If there are no cross terms between temporal and spatial errors, this should produce a constant temporal error for each calculation, which we presumed was significantly smaller than the spatial error.

Four physical quantities were calculated and analyzed for each problem. They were density, pressure, SIE, and either speed or x-velocity (for the 1-D test problem). Note that speed,

$$u = \sqrt{u_x^2 + u_y^2} \tag{24}$$

is a scalar quantity, not a vector. Four simulations of different zoning were run for each test problem. As the convergence analysis requires three simulations of different zoning, this resulted in two convergence calculations for each variable and each problem for calculation verification, and four convergence results in the two test problems for which code verification was conducted as well.[9]

Rigorously, the exact solution at the center of the computational cell should not be used to evaluate codes that employ the finite volume method, as does the RAGE code used in this study. Instead, the integrated average of the exact solution over the entire cell should be used. Previous experience and numerous calculations using the RAGE code suggest little difference in the convergence results between calculations using the exact solution at the zone center and calculations using the numerically estimated integral of the exact solution over the zone. Exact solutions were calculated to double machine precision.

A. A 2-D Linear Acoustic Wave Problem

The 2-D acoustic wave problem, described in detail in Ref. [18–20], is based on specific initial conditions for the 2-D Cartesian gas dynamics equations. When the amplitude of the initial conditions is sufficiently small, there exists a closed form solution that is asymptotically valid for early time. This closed form result involves the solution of a linear wave equation, so we refer to this configuration as the "linear" acoustic wave problem. The initial conditions for this problem consist of constant, uniform values of density, pressure, and velocity that have been given sinusoidal perturbations. The solution remains smooth for the times considered.

The problem we consider is defined on the unit square $\Omega \equiv \{(x, y) : (x, y) \in [0, 1] \times [0, 1]\}$ with periodic boundary conditions along the edge $\partial\Omega$. We prescribe the temporal dependence to be oscillatory with angular frequency ω. The wavevector $\boldsymbol{k} \equiv k_x\hat{x} + k_y\hat{y}$ governs both the direction and period of the spatial variation of the solution, where $\hat{x}$ and $\hat{y}$ are unit vectors. The closed-form solution for the specific problem we consider is given in Table 2, in which k represents the magnitude of the wavevector, i.e., $|\boldsymbol{k}|$, and ε is a small parameter relating the size of the perturbations to the size of the constant field variables.

Table 2 2-D linear acoustic wave initial conditions (IC) and exact solution.

Variable	Base IC $(\bullet)_0$	Perturbed IC $(\bullet)'$	Base solution $(\bullet)_0$	Perturbed solution $(\bullet)'$
u_x	0	$\varepsilon(k_x/k)\cos(k_x x + k_y y)$	0	$\varepsilon(k_x/k)\cos(k_x x + k_y y)\cos(\omega t)$
u_y	0	$\varepsilon(k_y/k)\cos(k_x x + k_y y)$	0	$\varepsilon(k_y/k)\cos(k_x x + k_y y)\cos(\omega t)$
ρ	1	0	1	$\varepsilon(\rho_0\omega/k)\sin(k_x x + k_y y)\sin(\omega t)$
p	3/10	0	3/10	$(\varepsilon/c_0^2)(\rho_0\omega/k)\sin(k_x x + k_y y)\sin(\omega t)$

The specific parameters used in the problem we consider are given in Table 3. With these parameters, the calculation was run from an initial time of $t = 0$ s to a final time of $t = 0.2$ s on meshes containing $50 \times 50, 100 \times 100, 200 \times 200$, and 400×400 zones on the unit square.

The global convergence results from a code verification analysis are summarized in Tables 4 and 5. The L_1 norm of the difference between the asymptotically exact solution and the computed solution over the various computational meshes is shown for each physical variable in addition to the exact global convergence rates. The theoretical value for these rates is two, indicating the set of rates for the 200 and 400 cell meshes is very low. A possible reason for this is that the temporal error (or other errors) was becoming significant in relation to the spatial error. Next, calculation verification was conducted on the data and an estimated solution was generated. The pointwise estimated solution was then used to calculate global convergence rates, shown in Table 6 and to be compared with the values in Table 5. The estimated convergence rates are higher, presumably because the estimated solution contains the temporal and zeroth-order errors, making the convergence appear faster than it really is.

Table 3 2-D linear acoustic wave initial parameters.

γ	k_x	k_y	ω	ε
5/3	2π	2π	2π	10^{-4}

Table 4 Exact global error for the 2-D linear acoustic wave: exact-computed L_1 errors.

Number of cells	$\Delta x = \Delta y$, cm	$\|\rho^* - \rho_{\Delta x}\|_1$, g/cm^3	$\|p^* - p_{\Delta x}\|_1$, dyne/cm^2	$\|e^* - e_{\Delta x}\|_1$, erg/g	$\|u^* - u_{\Delta x}\|_1$, cm/s
50	2.0×10^{-2}	2.81×10^{-7}	1.40×10^{-7}	8.43×10^{-8}	2.65×10^{-7}
100	1.0×10^{-2}	6.61×10^{-8}	3.31×10^{-8}	1.99×10^{-8}	7.95×10^{-8}
200	5.0×10^{-3}	1.62×10^{-8}	8.38×10^{-9}	5.48×10^{-9}	2.02×10^{-8}
400	2.5×10^{-3}	7.48×10^{-9}	4.70×10^{-9}	3.88×10^{-9}	5.68×10^{-9}

Table 5 Exact global convergence rate, q_g, for the 2-D linear acoustic wave.

Num of cells	$\Delta x = \Delta y$, cm	Density	Pressure	Energy	Speed
50, 100	$(2, 1) \times 10^{-2}$	2.09	2.08	2.08	1.73
100, 200	$(10, 5) \times 10^{-3}$	2.03	1.98	1.86	1.98
200, 400	$(5.0, 2.5) \times 10^{-3}$	1.11	0.833	0.496	1.83

Table 6 Estimated global convergence rate, q_g, for the 2-D linear acoustic wave.

$\Delta x = \Delta y$, cm, $\hat{\xi}$	$\Delta x = \Delta y$, cm, Calculation	Density	Pressure	Energy	Speed
$(20, 10, 5) \times 10^{-3}$	$(2, 1) \times 10^{-2}$	2.56	2.56	2.56	2.45
$(10, 5, 2.5) \times 10^{-3}$	$(10, 5) \times 10^{-3}$	2.67	2.67	2.67	2.46

Table 7 Exact-estimated solution error for the 2-D linear acoustic wave.

$\Delta x = \Delta y$, cm, $\hat{\xi}$	$\Delta x = \Delta y$, cm, Exact	$\|\rho^* - \hat{\rho}\|_1$, g/cm^3	$\|p^* - \hat{p}\|_1$, dyne/cm^2	$\|e^* - \hat{e}\|_1$, erg/g	$\|u^* - \hat{u}\|_1$, cm/s
$(20, 10, 5) \times 10^{-3}$	2.0×10^{-2}	1.25×10^{-7}	6.27×10^{-8}	3.76×10^{-8}	5.21×10^{-8}
$(10, 5, 2.5) \times 10^{-3}$	1.0×10^{-2}	3.12×10^{-8}	1.56×10^{-8}	9.37×10^{-9}	2.27×10^{-8}

The first two rows in Table 4 are to be compared with the values in Table 7, which displays the L_1 norm of the difference between the exact solution and the estimated solution. Fig. 1 graphically shows that the estimated solution is very close to the exact solution for this problem. Comparing the values in Tables 4 and 7 demonstrates that the estimated solution error is less than the computed solution error for the same grid, but more than the computed solution error for the fine grid. The left plot of Fig. 2 shows this graphically for pressure. The estimated solution is a function of zone size and its corresponding error consistently decreases with the zone size.

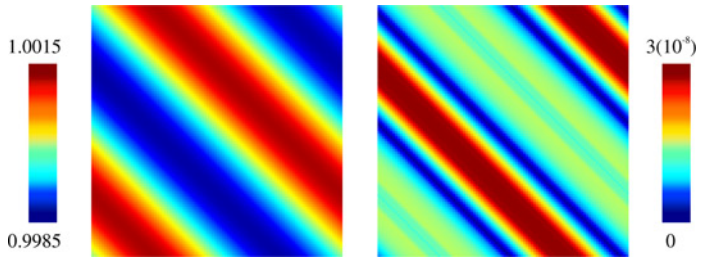

Fig. 1 Plots are shown of the 2-D linear acoustic wave problem's estimated pressure, $\hat{\xi}$, (left) and the difference between the exact and estimated pressure, $|\xi^* - \hat{\xi}|$, (right) in dyne/cm^2. Plots are shown at $t = 0.2$ s for a 100 × 100 mesh on the unit square. Initially, the pressure is 0.3 dynes/cm^2 uniformly and evolves into a sinusoidal wave with small perturbations around the initial condition. The estimated solution is within 0.001% of the exact solution for this problem.

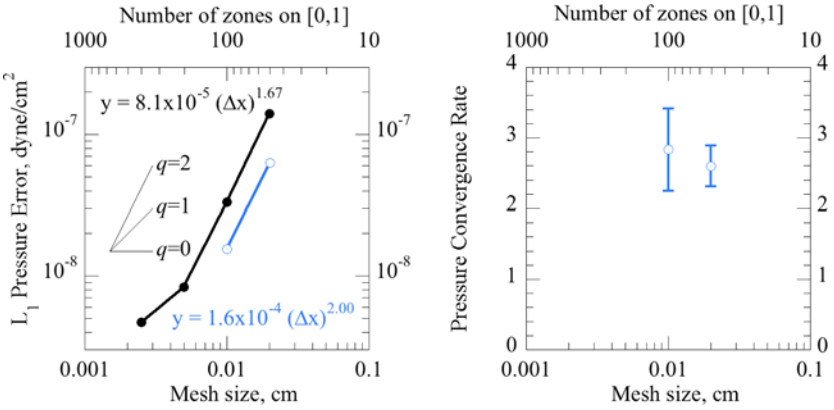

Fig. 2 Plots are shown for the 2-D linear acoustic wave problem. The black line in the left plot is the L_1 norm of the difference between the exact and the computed solutions for pressure, $|\xi^* - \xi_{\Delta x}|$. The blue line is the L_1 norm of the difference between the exact and the estimated solutions for pressure $|\xi^* - \hat{\xi}|$. The lines to the left of the L_1 norms represent convergence rates of $q = 0$, 1, and 2. The equations in the left plot give the effective convergence relation associated with each set of data points. The error in the estimated solution is approximately a factor of two smaller than the error in the corresponding RAGE solution. Plots of the mean pointwise convergence rate $q \pm$ one standard deviation are shown on the right. Time for both plots is 0.2 s.

The mean pointwise convergence rate and prefactor, A from Eqs. (17), were both found to increase with a decrease in zone size for all variables, which is the opposite behavior observed from the global quantities. The increase in mean convergence rate and its corresponding standard deviation is shown for pressure in Fig. 2. One possible explanation for the increase in the convergence quantities with zoning is that there may be a few points that changed dramatically as the zoning was decreased producing relatively large convergence values, while most points produced a decrease in the convergence values. This hypothesis is supported by the large increase in the standard deviation going from the coarse to fine values.

B. A 2-D Nonlinear Acoustic Wave Problem

The nonlinear acoustic wave problem is a more general case of the problem described in the previous section. Specifically, the domain, boundary conditions, and form of the initial conditions are the same. The problem we consider is specified by the parameters in Table 3 with the exception that that the magnitude of the perturbation was set to $\varepsilon = 0.01$. With these parameters, the nonlinear waves do not remain sinusoidal as in the linear case; rather, they become steeper and begin to resemble shocks. The calculation was run from an initial time of $t = 0$ s to a final time of $t = 0.2$ s.

The asymptotically exact solution of Table 2 is not valid in this case, so one cannot evaluate exact convergence parameters for this problem. We compared the results of the *nonlinear* simulations to the exact *linear* solution in order to make certain that the problem was indeed nonlinear. The difference was several orders of magnitude larger than for the 2-D linear acoustic wave problem, demonstrating that the problem was indeed no longer in the linear regime. The solution and effective error for speed in this problem are shown graphically in Figs. 3 and 4.

Tables 8 and 9 contain the global convergence results where the estimated solution is used to evaluate the error in the computed solution, as no exact solution is available. The problem demonstrates the utility of our approach when no exact solution is known. The estimated convergence rates are larger than the theoretical value of two for this problem.

Table 10 contains the mean and standard deviation of the pointwise convergence prefactor. The mean prefactor exhibits exceptionally large values in the fine zoning case for density, pressure and internal energy, but not for speed. We do not know why such anomalously large values are present in this problem. Very large prefactors are present in subsequent problems; however, in those cases the large values are due to regions of quiescent material, which is not present in the acoustic wave problems.

We have considered two hypotheses as to why the prefactors may be large. First, with small zoning, large prefactors result from large convergence rates. If the change in the physical quantities going from coarse to medium zoning is much larger than the change going from medium to fine zoning, then the convergence rate could be very large. Mean convergence rates for the nonlinear acoustic wave problem are close to three, but with a standard deviation of about one, suggesting exceptionally large convergence rates in some cells.

An alternative hypothesis is that there are spurious roots for the error model and the Newton solver sometimes converges to these roots instead of the appropriate solution. We hoped by starting the Newton solver close to the calculated solutions to only find the root of interest, but such is not guaranteed.

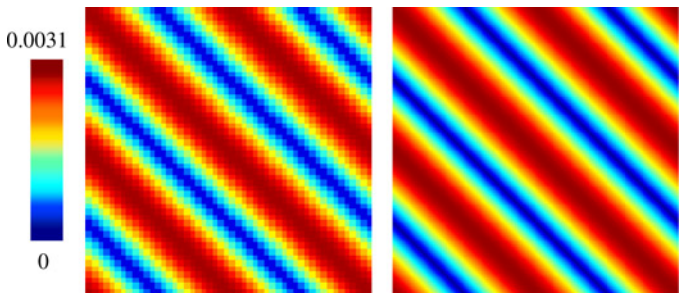

Fig. 3 Plots of the computed speed for the 2-D nonlinear acoustic wave problem at time 0.2 s on the 50 × 50 (left) and 400 × 400 (right) meshes on the unit square. All values are in cm/s. Recall that $0.0 \leq u \leq 0.01$ at $t = 0$.

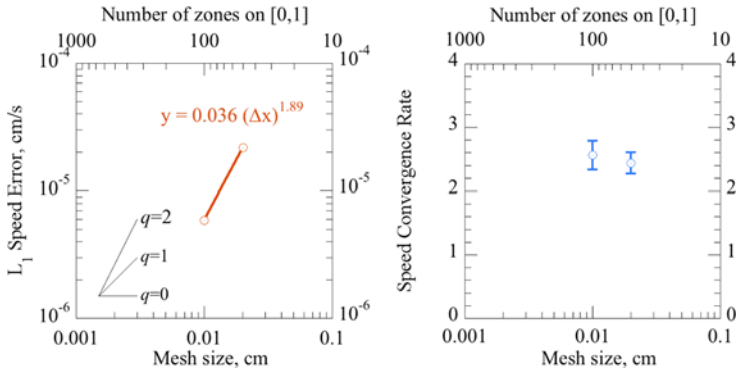

Fig. 4 The plot on the left shows the effective error, $|\hat{\xi} - \xi_{\Delta x}|$, in the speed for the 2-D nonlinear acoustic wave problem at time 0.2 s on the two computational meshes for which the estimated solution was obtained. Although it appears visually similar, this is a different kind of data than that shown in Figure 2. Lines in the lower left of the plot represent convergence rates of $q = 0$, 1, and 2. The equation gives the effective convergence relation associated with the two data points. The plot on the right shows mean convergence rates $q \pm$ one standard deviation.

Table 8 Estimated global error for the 2-D nonlinear acoustic wave; estimated-computed L_1 errors.

$\Delta x = \Delta y$, cm, $\hat{\xi}$	$\Delta x = \Delta y$, cm, Calculation	$\|\hat{\rho} - \rho_{\Delta x}\|_1$, g/cm^3	$\|\hat{p} - p_{\Delta x}\|_1$, dyne/cm^2	$\|\hat{e} - e_{\Delta x}\|_1$, erg/g	$\|\hat{u} - u_{\Delta x}\|_1$, cm/s
$(20, 10, 5) \times 10^{-3}$	2.0×10^{-2}	1.59×10^{-5}	7.96×10^{-6}	4.77×10^{-6}	2.18×10^{-5}
$(20, 10, 5) \times 10^{-3}$	1.0×10^{-2}	2.70×10^{-6}	1.35×10^{-6}	8.10×10^{-7}	4.05×10^{-6}
$(10, 5, 2.5) \times 10^{-3}$	1.0×10^{-2}	3.84×10^{-6}	1.92×10^{-6}	1.15×10^{-6}	5.88×10^{-6}
$(10, 5, 2.5) \times 10^{-3}$	5.0×10^{-3}	6.01×10^{-7}	3.01×10^{-7}	1.80×10^{-7}	1.07×10^{-6}

Table 9 Estimated global convergence rate, q_g, for the 2-D nonlinear acoustic wave.

$\Delta x = \Delta y$, cm, $\hat{\xi}$	$\Delta x = \Delta y$, cm, Calculation	Density	Pressure	Energy	Speed
$(20, 10, 5) \times 10^{-3}$	$(2, 1) \times 10^{-2}$	2.56	2.56	2.56	2.43
$(10, 5, 2.5) \times 10^{-3}$	$(10, 5) \times 10^{-2}$	2.68	2.67	2.68	2.46

Table 10 Estimated, pointwise convergence coefficient, A, for the 2-D nonlinear acoustic wave.

$\Delta x = \Delta y$, cm, $\hat{\xi}$	$\Delta x = \Delta y$, cm, A	Density	Pressure	SIE	Speed
$(20, 10, 5) \times 10^{-3}$	2.0×10^{-2}	0.938 ± 1.94	0.470 ± 0.977	0.281 ± 0.579	0.334 ± 0.224
$(10, 5, 2.5) \times 10^{-3}$	1.0×10^{-2}	$(3.89 \pm 27.3) \times 10^{11}$	$(3.46 \pm 24.3) \times 10^{10}$	$(2.00 \pm 14.0) \times 10^{9}$	0.736 ± 0.391

C. A 1-D Riemann Problem

Unlike the smooth solutions of the two acoustic problems, solutions to the two Riemann problems involve discontinuities. We consider the case in which a rarefaction fan, a contact discontinuity, and a shock wave develop. The initial conditions for the case we consider are given in Table 11, with $\gamma = 1.4$.

This problem was run on the domain $0 < x < 1$, with meshes of 20, 40, 80, and 160 zones. The exact solution was computed using an algorithm based on Ref. [21]. The solutions were compared at a single time of $t = 0.2$ s.

Tables 12 and 13 show the convergence for this problem using an exact solution, while Table 14 shows the global convergence rates using an estimated solution. For comparison, the theoretical convergence value is unity. Again, as in the linear acoustic wave problem, the estimated convergence rates are much higher than the exact values. The error of the estimated solution (on the course mesh), shown in Table 15, is smaller than the error of the computed

Table 11 Initial conditions for the 1-D Riemann problem.

Position	ρ, g/cm^3	p, dyne/cm^2	e, erg/g	u, cm/s
$0.0 < x < 0.5$	1.00	1.00	2.50	0.000
$5 < x < 1.0$	2.25	1.80	2.00	0.00

Table 12 Exact global error for the 1-D Riemann problem; exact-computed L_1 errors.

Number of cells, [0,1]	Δx, cm	$\|\rho^* - \rho_{\Delta x}\|_1$, g/cm^3	$\|p^* - p_{\Delta x}\|_1$, dyne/cm^2	$\|e^* - e_{\Delta x}\|_1$, erg/g	$\|u_x^* - u_{x\Delta x}\|_1$, cm/s
20	5.0×10^{-2}	4.10×10^{-2}	3.59×10^{-2}	3.73×10^{-2}	2.18×10^{-2}
40	2.5×10^{-2}	2.59×10^{-2}	2.11×10^{-2}	2.32×10^{-2}	1.24×10^{-2}
80	1.25×10^{-2}	1.59×10^{-2}	1.2×10^{-2}	1.43×10^{-2}	7.29×10^{-3}
160	6.25×10^{-3}	9.25×10^{-3}	6.28×10^{-3}	9.63×10^{-3}	3.72×10^{-3}

Table 13 Exact global convergence rate, q_g, for the 1-D Riemann problem.

Num of cells	Δx, cm	Density	Pressure	SIE	x-Velocity
20, 40	$(5, 2.5) \times 10^{-2}$	0.660	0.767	0.680	0.817
40, 80	$(2.5, 1.25) \times 10^{-2}$	0.709	0.808	0.705	0.766
80, 160	$(12.5, 6.25) \times 10^{-3}$	0.778	0.940	0.567	0.968

Table 14 Estimated global convergence rate, q_g, for the 1-D Riemann problem.

Δx, cm, $\hat{\xi}$	Δx, cm, Calculation	Density	Pressure	SIE	x-Velocity
$(5, 2.5, 1.25) \times 10^{-2}$	$(5, 2.5) \times 10^{-2}$	1.62	1.74	1.63	1.80
$(25, 12.5, 6.25) \times 10^{-3}$	$(2.5, 1.25) \times 10^{-2}$	1.68	1.76	1.71	1.76

Table 15 Exact-estimated solution error for the 1-D Riemann problem.

Δx, cm, $\hat{\xi}$	Δx, cm, Exact	$\|\rho^* - \hat{\rho}\|_1$, g/cm^3	$\|p^* - \hat{p}\|_1$, dyne/cm^2	$\|e^* - \hat{e}\|_1$, erg/g	$\|u_x^* - \hat{u}_x\|_1$, cm/s
$(5, 2.5, 1.25) \times 10^{-2}$	5.0×10^{-2}	1.97×10^{-2}	1.62×10^{-2}	1.78×10^{-2}	9.95×10^{-3}
$(25, 12.5, 6.25) \times 10^{-3}$	2.5×10^{-2}	1.28×10^{-2}	9.52×10^{-3}	1.14×10^{-2}	5.90×10^{-3}

solution on the same course grid, but, as in the acoustic wave problem, larger than the error of the fine computational solution evaluated on the fine mesh.

Plots of the exact and computed solutions at this time are given in Fig. 5. Note that x-velocity is used in this problem in place of speed. Fig. 5 compares the exact solution to this problem for SIE with the computational solution for 20 zones. A rarefaction is seen moving to the right, a shock wave to the left, and a contact discontinuity in the center. Not surprisingly, the error between the exact and calculated solutions is concentrated at the locations of the three discontinuities. The estimated solution is seen to match the exact solution more accurately than the computed solution.

Significantly, the convergence results may be used to approximate the computational error. The dashed red lines around the calculated solution correspond to the quantity $\pm A\Delta x^q$ about those values. The dashed lines give a sense of the magnitude of error in the computed solution, especially in cases when there is no exact solution. Notice that the dashed lines from the error model *do not* always encompass the exact solution; however, they do indicate where the error is greatest.

Figure 5 also shows a comparison of the L_1 norm of the exact-calculated error with the L_1 norm of the estimated-calculated error. In cases where the exact solution is unknown, the estimated solution may be used. Fig. 5 shows for this problem that use of the estimated solution gives somewhat different results than the exact solution. Such a result

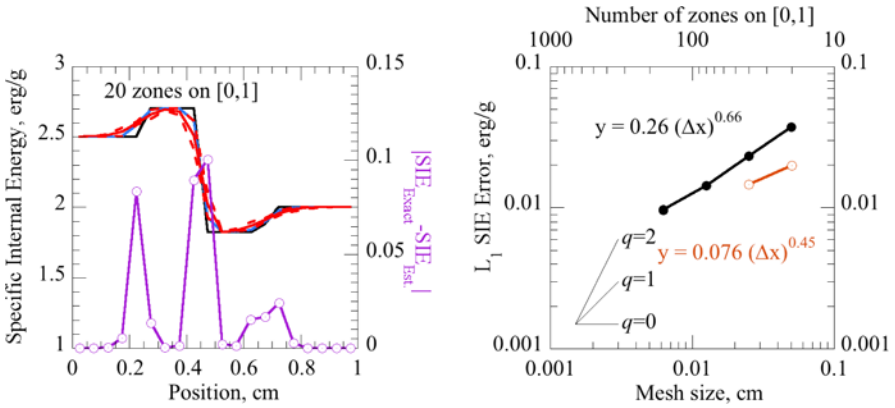

Fig. 5 Both plots are for the SIE of the 1-D Riemann problem on the 20-zone computational mesh at a time of 0.2 s. The exact solution on this mesh (in black), the estimated solution (in blue), and the calculated solution (in red) are plotted against the left ordinate, while the difference between these solutions (in purple) is plotted against the right ordinate. The dashed lines (in red) indicate values that are $\pm A\Delta x^q$ relative to the calculated solution. The plot on the right shows the L_1 norm of the difference between the exact and the computed solution for the SIE, $|\xi^* - \xi_{\Delta x}|$, (in black). The effective error, $|\hat{\xi} - \xi_{\Delta x}|$ is shown in orange for comparison. The lines in the lower left of the plot represent convergence rates of $q = 0$, 1, and 2. The equations give the effective convergence relation associated with each set of data points.

does not preclude use of the estimated solution for error analysis in cases where there is no exact solution, but it does seem to advise caution.

The convergence rates for all physical quantities on this problem varied between 0.66–0.97, which is consistent with the theoretical maximum of unity[22,23] as well as previous experience on convergence analysis for problems containing shocks. Figure 6 shows values of the convergence rate and prefactor for SIE. The variation of the convergence rate in Fig. 6 is not oscillatory convergence. In order to calculate the convergence of each point in Fig. 6, three calculations were run, which, at each point, could have converged monotonically, in an oscillatory manner, or not at all.

The convergence rates and prefactor become very large at the edges of the plots, as was previously seen in the nonlinear acoustic wave problem, but for a different reason in this case. The edges of the plots correspond to quiescent regions: with little or no change in the computational results such large values can be observed. The large values for both the prefactor and convergence rate in the quiescent regions are not real, rather a spurious artifact of the

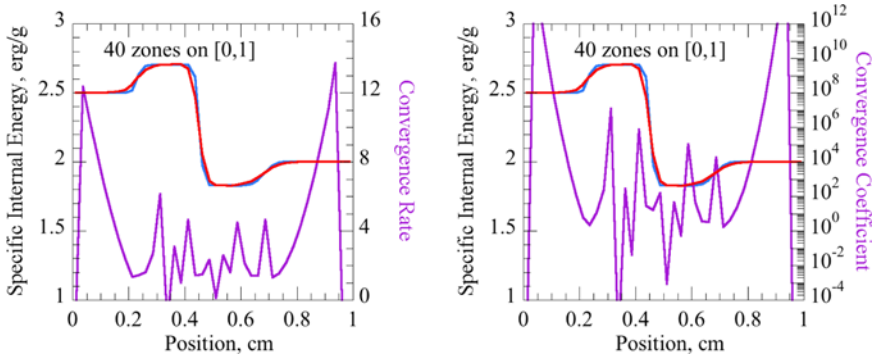

Fig. 6 Plots of the estimated pointwise convergence rate q (left) and prefactor A (right) for SIE are shown for the 1-D Riemann problem estimated from the 40-, 80-, and 160-zone computational meshes at a time of 0.2 s. The estimated solution (in blue) and the computed solution (in red) are plotted against the left ordinate, while the pointwise convergence rate (in purple) is plotted against the right ordinate.

convergence analysis. Likewise, the values showing negative convergence rates are an artifice used to designate areas of the mesh for which no convergence could be calculated, i.e., there was no actual negative convergence.

All the physical quantities, not just the SIE, showed large convergence rates and prefactors at the edges. The large values resulted in overly large mean values and large standard deviations for both the convergence rates and prefactors. One way to ameliorate to this problem of data pollution from quiescent regions would be to include a filter when averaging the convergence rates and prefators, such that only cells that contribute significantly to the error would be included in the average.

D. A 2-D Riemann Problem

The 2-D Riemann problem is a natural extension of the previous case. Although there is no known exact solution, numerical evidence suggests that 19 fundamentally different patterns or types of structures can develop for the 2-D Riemann problem for a polytropic gas.[23–26] We consider one of the all-rarefaction cases in our analysis. The domain of interest is the unit square $\Omega \equiv \{(x, y) : (x, y) \in [0, 1] \times [0, 1]\}$; the full computational domain, however, is $\bar{\Omega} \equiv \{(x, y) : (x, y) \in [-1, 2] \times [-1, 2]\} \supset \Omega$, so that effects of the computational boundary $\partial\bar{\Omega}$ do not influence the calculated solution in Ω at the time of interest. With the four initial regions of the domain of interest numbered I–IV counter-clockwise from the upper right (i.e., $\mathrm{I} \equiv \{(x, y) : x > 0.5 \text{ and } y > 0.5\}$, $\mathrm{II} \equiv \{(x, y) : x \leq 0.5 \text{ and } y > 0.5\}$, etc.), the initial conditions for this problem are given in Table 16. The meshes we consider had 32×32, 64×64, 128×128, and 256×256 cells in them. We evaluate the solution at the final time of $t = 0.2$ s, as in Ref. [24].

As there is no exact solution, Tables 17 and 18 show the global convergence rates calculated using the estimated solution. The theoretical value is unity and so the convergence rates are high, consistent with the high values for estimated convergence in the other test problems. Significantly, a number of points were observed to converge in an oscillatory fashion and contributed to the values shown in Tables 17 and 18.

Figure 7 shows the estimated density for this problem and a corresponding map of the convergence index for the 64×64 mesh. The estimated density is qualitatively evocative of the plots in Ref. [24]. The convergence index shows graphically the convergence of points within the Newton solver. Newton's method is seen to have converged on almost all computational cells, only failing to converge on one cell due to problems with the algorithm. There is

Table 16 Initial conditions for the 2-D Riemann problem.

Region	ρ, g/cm^3	p, dyne/cm^2	e, erg/g	u_x, cm/s	u_y, cm/s
I	1.0	1.0	2.5	0.0	0.0
II	0.5197	0.4	1.9242	−0.7259	0.0
III	0.1072	0.0439	1.0238	−0.7259	1.4045
IV	0.2579	0.15	1.4541	0.0	−1.4045

Table 17 Estimated global error for the 2-D Riemann problem; estimated-computed L_1 errors.

$\Delta x = \Delta y$, cm, $\hat{\xi}$	$\Delta x = \Delta y$, cm, Calculation	$\|\hat{\rho} - \rho_{\Delta x}\|_1$, g/cm^3	$\|\hat{p} - p_{\Delta x}\|_1$, dyne/cm^2	$\|\hat{e} - e_{\Delta x}\|_1$, erg/g	$\|\hat{u} - u_{\Delta x}\|_1$, cm/s
$(31.25, 15.625, 7.8125) \times 10^{-3}$	3.125×10^{-2}	8.77×10^{-3}	8.79×10^{-3}	3.69×10^{-2}	2.01×10^{-2}
$(31.25, 15.625, 7.8125) \times 10^{-3}$	1.5625×10^{-2}	2.84×10^{-3}	2.59×10^{-3}	1.07×10^{-2}	6.03×10^{-3}
$(15.625, 7.8125, 3.90625) \times 10^{-3}$	1.5625×10^{-2}	5.70×10^{-3}	4.92×100^{-3}	2.02×10^{-2}	1.14×10^{-2}
$(15.625, 7.8125, 3.90625) \times 10^{-3}$	7.8125×10^{-3}	1.68×10^{-3}	1.42×10^{-3}	5.63×10^{-3}	3.24×10^{-3}

Table 18 Estimated global convergence rate, q_g, for the 2-D Riemann problem.

$\Delta x = \Delta y$, cm, $\hat{\xi}$	$\Delta x = \Delta y$, cm, Calculation	Density	Pressure	Energy	x-Velocity
$(31.25, 15.625, 7.8125) \times 10^{-3}$	$(3.125, 1.5625) \times 10^{-2}$	1.63	1.76	1.79	1.74
$(15.625, 7.8125, 3.90625) \times 10^{-3}$	$(15.625, 7.8125) \times 10^{-3}$	1.76	1.79	1.84	1.81

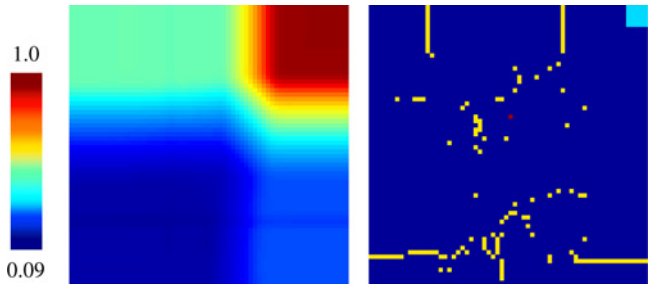

Fig. 7 Plots of the estimated density (left) and the Newton solver convergence index (right) are shown for the 2-D Riemann rarefaction problem at time 0.2 s on the 64 × 64 mesh on the unit square. The values for density are in g/cm^3. Newton solver convergence index key: (1) Blue : Newton solver converged. (2) Light Blue: Points with an order for which no solution exists. (3) Gold: Points too close together to calculate convergence reliably. (4) Red: A zero was in the diagonal of the U matrix and the Newton solver failed.

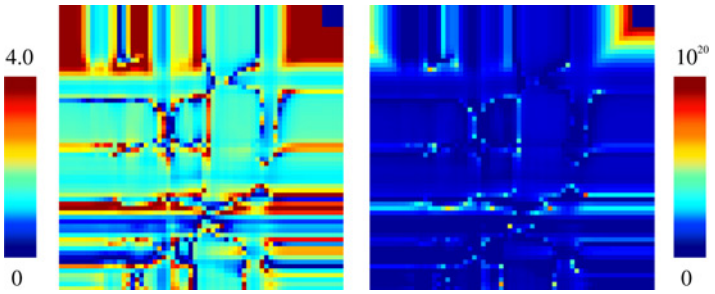

Fig. 8 Plots of the density convergence rate q (left) and prefactor A (right) for the 2-D Riemann rarefaction problem from the 64-, 128-, and 256-zone computational meshes at time 0.2 s. The prefactor is plotted logarithmically. It is seen that the method converged at very high rates in the upper right and left corners and along a horizontal band about a quarter of the way up from the bottom. The upper corners were quiescent regions while the band at the bottom of the figures corresponds to start up error.

a significant number of cells for which convergence was not possible. Part of the quiescent region of the problem in the upper right hand corner produced no change in the physical quantities, and so was impossible to compute convergence for. Likewise, it was impossible to calculate convergence in cells for which differences in the solution fell below some user specified tolerance.

A map of the convergence rates and prefactors for density is shown in Fig. 8. Exceptionally high values of each are concentrated in the area of quiescence at the top right corner of the computational mesh. As with the 1-D Riemann problem, the large values for the convergence and prefactor are spurious. Convergence cannot be accurately calculated in a region of quiescence. The quiescent region contributes little to the computational error; a more accurate measure of the mean prefactor and convergence rate would exclude the large values found in the quiescent region.

Close observation of the maps shows a distinct horizontal band of high convergence and prefactor values running about a third of the way up from the bottom of the plot. This band is believed to be the result of start-up errors, associated with the initial conditions of the problem.

V. Summary and Conclusions

We have described, implemented, and applied a method by which to approximate global convergence when an exact solution is unavailable by using an estimated solution in place of an exact solution. Because the estimated solution is pointwise and determined from mesh convergence analysis, obtaining convergence rates for as many points in the mesh as possible is desired in order to have as complete an estimated solution as possible. Calculating

local oscillatory convergence as well as monotonic convergence is therefore useful, especially in problems with discontinuities.

We have evaluated this process on a small set of simple 1-D and 2-D test problems, both smooth and non-smooth. The problems were a 2-D linear acoustic wave, a 2-D nonlinear acoustic wave, a 1-D Riemann problem, and a 2-D Riemann problem. Simulations were conducted with the RAGE code and a simple error model. All computational grids were uniform and a constant, fixed time step was used.

In the two problems with exact solutions, a direct comparison could be made between estimated and exact convergence rates. The estimated rates were consistently higher than the exact rates, presumably because the estimated solution contained temporal and zeroth-order errors not accounted for in our simple error model. If one used a better error model, the difference between exact and estimated convergence rates could be smaller.

Another interesting observation has to do with the error of the estimated solution. The estimated solution is calculated on the coarse grid of three computational solutions, one on a coarse, one on a medium, and one on a fine grid. The estimated solution evaluated on the coarse grid was shown to be more accurate than the coarse computational solution. It was not as accurate as the fine computational solution evaluated on the fine grid. We observed a few chosen points and compared the error of the estimated solution to the fine computational solution, both evaluated on the coarse grid, and found that they were much closer, but that the fine computational solution still had slightly less error. A natural question is whether it wouldn't be better to simply use the fine computational solution as a stand-in for the exact solution under such circumstances. One would expect the estimated solution should be superior to the fine grid solution as the estimated solution contains mathematical information regarding the computational error. A more accurate error model might yield an estimated solution that is superior to the fine computational solution; however, the results of this study indicate that one should be cautious. A discussion of the reasons for using a simple error model was presented in § 2.

Lastly, the method did successfully calculate pointwise oscillatory convergence for some points in the 2-D Riemann problem. The convergence of these points was used to construct a more complete estimated solution and thereby a more meaningful global convergence rate.

Acknowledgments

This work was performed by Los Alamos National Laboratory, which is operated by the University of California for the National Nuclear Security Administration of the U.S. Department of Energy under contract W-7405-ENG-36. The document is available as Los Alamos National Laboratory Report LA-UR-06-2006. The authors acknowledge the kind support of the LANL ASC V& V Program and its manager, Scott Doebling. We appreciate the ongoing and stimulating technical interactions on verification-related issues with our Verification Project team members, in particular, François Hemez and Bill Rider. The constructive and insightful feedback of these colleagues on early drafts of this paper is gratefully acknowledged.

References

[1]*AIAA Guide for the Verification and Validation of Computational Fluid Dynamics Simulations*, AIAA Guide G-077-1998, 1998.

[2]Knupp, P. and Salari, K., *Verification of Computer Codes in Computational Science and Engineering*, Chapmann and Hall/CRC Press, Boca Raton, FL, 2003.

[3]Oberkampf, W. L., Trucano, T. G., and Hirsch, C., "Verification, validation, and predictive capability in computational engineering and physics", *Applied Mechanics Reviews*, Vol. 57, No. 5, Sept. 2004, pp. 345–384.

[4]Roache, P. J., "Quantification of Uncertainty in Computational Fluid Dynamics", *Annual Review of Fluid Mechanics*, Vol. 29, 1997, pp. 123–160.

[5]Roache, P. J., *Verification and Validation in Computational Science and Engineering*, Hermosa Publishers, Albuquerque, NM, 1998.

[6]Roy, C. J., "Review of code and solution verification procedures for computational simulation", *Journal of Computational Physics*, Vol. 205, No. 1, 1 May 2005, pp. 131–156.

[7]Cadafalch, J., Pérez-Segarra, C. D., Còsul, R., and Oliva, A., "Verification of Finite Volume Computations on Steady-State Fluid Flow and Heat Transfer", *Journal of Fluids Engineering*, Vol. 24, No. 1, March 2002, pp. 11–21.

[8]Stern, F., Wilson, R., and Shao, J., "Quantitative V& V of CFD simulations and certification of CFD codes", *International Journal of Numerical Methods for Fluids*, Vol. 50, No. 11, 20 April 2006, pp. 1335–1355.

[9]Smitherman, D. P., Kamm, J. R., and Brock, J. S., "Calculation Verification: Pointwise Estimation of Solutions and Their Method Associated Numerical Error", Los Alamos National Laboratory Report LA-UR-05-8002, 2005.

[10]Li, S., Rider, W.J., and Shashkov, M.J., "Two-Dimensional Convergence Study for Problems with Exact Solution: Uniform and Adaptive Grids", Los Alamos National Laboratory Report LA-UR-05-7985, 2005.

[11]Brock, J. S., "Isolating Temporal-Discretization Errors for Separate-Verification Analysis", *42^{nd} AIAA Aerospace Sciences Meeting and Exhibit*, Reno, NV, Paper No. AIAA-2004-0741, Jan. 2004, pp. 8546-8556. Los Alamos National Laboratory Report LA-UR-03-9160, 2003.

[12]Hemez, F. M., Brock, J. S., and Kamm, J. R., "Non-linear Error Ansatz Models in Space and Time for Solution Verification", *Proceedings of the 47^{th} AIAA/ASME/ASCE/AHS/ASC Structures, Structural Dynamics, and Materials (SDM) Conference* and *1^{st} Non-deterministic Approaches (NDA) Conference*, Newport, RI, May 2006, *AIAA Meeting Papers on Disc* [CD-ROM], CD Code 1172-249678, Paper No. AIAA-2006-1995. Los Alamos National Laboratory Report LA-UR-06-3705, 2006.

[13]Kamm, J. R., Rider, W. J., and Brock, J. S., "Combined Space and Time Convergence Analysis of a Compressible Flow Algorithm", *16^{th} AIAA Computational Fluid Dynamics Conference*, Orlando, FL, Paper No. AIAA-2003-4241, July 2003. Los Alamos National Laboratory Report LA-UR-03-2628, 2003.

[14]Timmes, F. X., Fryxell, B. A., and Hrbek, G. M., "Spatial-temporal convergence properties of the Tri-Lab Verification Test suite in 1D for code project A", Los Alamos National Laboratory Report LA-UR-06-6444, 2006.

[15]Press, W. H., Teukolsky, S. A., Vetterling, W. T., and Flannery, B. P., *Numerical Recipes in FORTRAN: The Art of Scientific Computing*, 2^{nd} ed., Cambridge University Press, New York, NY, 1992, p. 372.

[16]Press, W. H., Teukolsky, S. A., and Vetterling, W. T., Flannery, B.P., *Numerical Recipes in FORTRAN: The Art of Scientific Computing*, 2^{nd} ed., Cambridge University Press, New York, NY, 1992, p. 376.

[17]Baltrusaitis, R. M., Gittings, M. L., Weaver, R. P., Benjamin, R. P., and Budzinski, J. M., "Simulation of shock-generated instabilities", *Physics of Fluids*, Vol. 8, No. 9, Sept. 1996, pp. 2471–2483.

[18]Kamm, J. R., Brock, J. S., Rousculp, C. L., and Rider, W. J., "Verification of an ASCI Shavano Project Hydrodynamics Algorithm", Los Alamos National Laboratory Report LA-UR-03-6999, 2003.

[19]Landau, L. D., and Lifschitz, E. M., *Fluid Mechanics*, Butterworth-Heinemann, Oxford and Boston, 1987.

[20]Whitham, G. B., *Linear and Nonlinear Waves*, John Wiley & Sons, New York, NY, 1974.

[21]Gottlieb, J. J. and Groth, C. P. T., "Assessment of Riemann solvers for unsteady one-dimensional inviscid flows of perfect gases", *Journal of Computational Physics*, Vol 78, No. 2, Oct. 1988, pp. 437–458.

[22]Kimoto, P. A. and Cherno, D. F., "Convergence Properties of Finite-difference Hydrodynamics Schemes in the Presence of Shocks", *Astrophysical Journal Supplemental Series*, Vol. 96, No. 2, Feb. 1995, pp. 627–641.

[23]Engquist, B. and Sjögreen, B., "The Convergence Rate of Finite Difference Schemes in the Presence of Shocks", *SIAM Journal of Numerical Analysis*, Vol. 35, No. 6, Dec. 1998, pp. 3464–2485.

[24]Lax, P. D. and Liu, X. D., "Solution of Two-Dimensional Riemann Problems of Gas Dynamics by Positive Schemes", *SIAM Journal of Scientific Computing*, Vol 19, No. 2, March 1998, pp. 319–340.

[25]Schulz-Rinne, C. W., "Classification of the Riemann Problem for Two-dimensional Gas Dynamics", *SIAM Journal of Mathematical Analysis*, Vol. 24, No. 1, Jan. 1993, pp. 76–88.

[26]Schulz-Rinne, C. W., Collins, J. P., and Glaz, H. M., "Numerical Solution of the Riemann Problem for Two-dimensional Gas Dynamics", *SIAM Journal of Scientific Computing*, Vol. 14, No. 6, Nov. 1993, pp. 1394–1414.

Jubaraj Sahu
Associate Editor